

Combustion Mechanisms of Spray Flat Flames Stabilized in a Laminar Counterflow

*Fumiteru AKAMATSU, Hiroyasu SAITOH, and Masashi KATSUKI
Department of Mechanical Engineering, Osaka University
2-1 Yamadaoka, Suita, Osaka 565-0871, Japan

ABSTRACT

Numerical calculations of n-decane polydisperse spray flames stabilized in a laminar two-dimensional counterflow configuration were conducted by the Eulerian/Lagrangian approach. For the gaseous phase, the Navier-Stokes equation together with mass, energy and species conservation equations was solved based on the finite control volume method with the SIMPLE algorithm. Transport properties and thermodynamic data of the gaseous species were obtained by CHEMKIN. For the disperse phase, all the individual droplets were tracked without using a concept of the *droplet parcel*. The film theory was employed for estimating a droplet evaporation rate and heat transferred from the gaseous phase to a droplet. As a result, it was found that twin flames of premixed combustion of pre-vaporized fuel and diffusion combustion of droplet groups were observed on the spray flow side and that the combustion intensity of the twin flames are different significantly depending on the droplet size distributions. This is mainly caused by the fact that prevaporization of fuel prior to combustion varies markedly depending on the droplet size distribution.

Key Words: Spray Combustion, Flame Structure, Numerical Simulation, Film Theory

INTRODUCTION

To build up a comprehensive model of spray combustion, more precise comparison of experimental observations and numerical calculation results is essential. However, due to lack of experimental information, most of spray combustion models in the past did not always reflect real physics of spray combustion. Therefore, it is necessary to build a spray combustion model based on the physics with deep communication between experimental and numerical researches.

In early 1970's, Chiu et al., proposed the droplet group combustion theory⁽¹⁾ in which droplet collective effect on the flame structure was taken into account. We have shown recently the quantitative experimental verification of the droplet group combustion by using spatially and temporally resolved multi-component data of combustion reactions and spray characteristics⁽²⁻⁴⁾ in stead of the ordinary time-averaged data. The experiments revealed that spray flames have much more complicated structure than they were modeled in the initial version of the droplet group combustion. Spatial nonuniformity of spray tends to form droplet groups, and temporal and spatial variations of their behavior generate the change in flame structure.

For numerical simulations of turbulent spray flames, the droplet parcel is frequently used to reduce the calculation load for tracking droplets in the flow field. The droplet collective effect, that is, droplet group combustion, cannot be taken into account correctly with this model. Adding to the fact above, turbulence model, turbulent combustion model and spray model are commonly used simultaneously to close Reynolds-averaged governing equations for the gas phase. Since the turbulence model is originally developed for single-phase isothermal flows, it is doubtful that the calculated effective viscosity ($\mu_{eff} = \mu_i + \mu_t$) can

be reasonably applied to combusting two-phase flows. The turbulent combustion model, represented by Reynolds averaged solutions of temperature and compositions, does contain a great deal of incorrectness. Moreover, the turbulent Schmidt/Prandtl numbers assumed as empirical constants are used in the calculation of mass and heat transport. Accordingly, in turbulent spray flame simulations where all of these uncertainties are incorporated, it is impossible to judge the validity of a new spray model and to optimize the model parameters, comparing the corresponding experimental result.

In the present study, numerical calculations of polydisperse spray flames were conducted in a laminar flow without use of the droplet parcel approximation, turbulence model and turbulent combustion model. Navier-Stokes equation, together with time-dependent mass, energy and species conservation equations was solved for the gaseous phase, considering the temperature dependence of transport properties and thermodynamic data of the gaseous species. For the disperse phase, all the individual droplets were tracked without using the concept of *droplet parcel*. The film theory was employed for estimating a droplet evaporation rate and heat transferred from the gaseous phase to a droplet. Detailed flame structure influenced by the spray characteristics was discussed.

CALCULATION METHOD

The planar two-dimensional flow field for the calculation is shown in Fig. 1. The origin of the calculation domain was located at the center of the upper rectangular burner port, from which liquid fuel, n-decane ($C_{10}H_{22}$) was supplied. The geometry of the burner port was 20 mm in width and the port separation was 20 mm. From the upper and lower burner ports, atmospheric air ($T=300$ K, oxygen mass fraction $Y_{O_2} = 0.2357$) was issued at the velocity of 0.4 m/s. Stretch ratio of the counter flow is 40 1/s. Polydisperse n-decane spray was injected from the upper port in the region of $0 \leq y \leq 3mm$ at the velocity of 0.4 m/s. The fuel-air mass ratio of the central ($0 \leq y \leq 3mm$) premixed spray was $0.051 \text{ kg}_{fuel}/\text{kg}_{air}$, which corresponds to nominal bulk equivalence ratio, $\phi_t = 0.75$. Droplet size distribution used for the calculation is shown in Fig. 2 (a) and (b). These were obtained by PDA measurement in our previous experiment^(5,6) in the non-reacting conditions. The initial position of droplet was determined by stochastic processes to generate a uniform spray flow in the region of $0 \leq y \leq 3mm$ of the upper port. Gaseous species considered

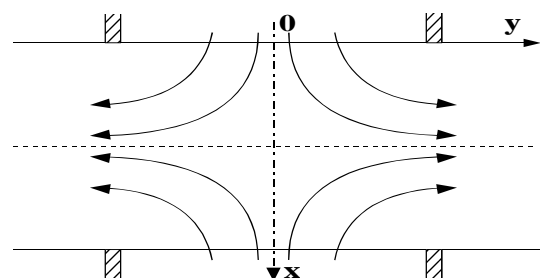


Fig. 1 Schematic of the flow field.

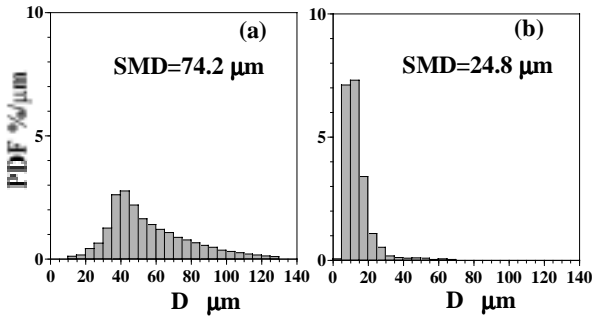


Fig. 2 The assumed droplet size distributions^(5,6).

in the calculations were O₂, N₂, CO₂, H₂O, and C₁₀H₂₂. Their transport properties and thermodynamic data were obtained by CHEMKIN^(7,8). Properties of liquid n-decane were obtained from the Ref. (9). The governing equations considered for the gaseous phase were mass, momentum, energy, and species mass conservation.

$$\frac{\partial \rho}{\partial t} + \frac{\partial \rho u}{\partial x} + \frac{\partial \rho v}{\partial y} = S_{l,m} \quad (1)$$

$$\frac{\partial \rho u}{\partial t} + \frac{\partial}{\partial x}(\rho u u - \mu \frac{\partial u}{\partial x}) + \frac{\partial}{\partial y}(\rho v u - \mu \frac{\partial u}{\partial y}) = -\frac{\partial P}{\partial x} + \frac{\partial}{\partial x} \mu \frac{\partial u}{\partial x} + \frac{\partial}{\partial y} \mu \frac{\partial u}{\partial y} + \rho g + S_{l,u} \quad (2)$$

$$\frac{\partial \rho v}{\partial t} + \frac{\partial}{\partial x}(\rho u v - \mu \frac{\partial v}{\partial x}) + \frac{\partial}{\partial y}(\rho v v - \mu \frac{\partial v}{\partial y}) = -\frac{\partial P}{\partial y} + \frac{\partial}{\partial x} \mu \frac{\partial v}{\partial x} + \frac{\partial}{\partial y} \mu \frac{\partial v}{\partial y} + S_{l,v} \quad (3)$$

$$\frac{\partial \rho h}{\partial t} + \frac{\partial}{\partial x}(\rho u h - \rho a \frac{\partial h}{\partial x}) + \frac{\partial}{\partial y}(\rho v h - \rho a \frac{\partial h}{\partial y}) = S_{l,h} \quad (4)$$

$$\frac{\partial \rho Y_k}{\partial t} + \frac{\partial}{\partial x}(\rho u Y_k - \rho D_k \frac{\partial Y_k}{\partial x}) + \frac{\partial}{\partial y}(\rho v Y_k - \rho D_k \frac{\partial Y_k}{\partial y}) = S_{comb,k} + S_{l,Y_k} \quad (5)$$

where ρ is gaseous phase density, u and v gaseous phase velocity in the x and y direction, respectively, μ viscosity, P static pressure, g gravitational acceleration, h specific total enthalpy, a thermal diffusivity, Y_k and D_k are mass fraction and mass diffusion coefficient of k 's species, respectively. $S_{comb,k}$ is the source term with the combustion. $S_{l,\ell}$ was considered to take interaction between the gaseous and disperse droplet phases into account. The gaseous phase density, ρ , is calculated from the state equation of the ideal gas. These governing equations were discretized by the finite volume method using the SIMPLE algorithm⁽¹⁰⁾ for solving the static pressure.

Mass, heat and momentum interchanges between the gaseous and disperse phases were calculated by a method of the PSI-Cell model⁽¹¹⁾ in which all interactions are evaluated on the basis of the gaseous phase calculation grids and its control volume. Interaction terms between the phases during a calculation time step are assumed to be concentrated at a control volume of the droplet final location of the time step. The followings are assumptions for the droplets.

- (1) No collision and no breakup of droplets occur.
- (2) Droplets are spherical and have uniform internal properties.
- (3) Volume of droplets is negligible.

The interaction terms between the gaseous and disperse phases were calculated explicitly regardless the implicit calculation of the gaseous phase.

The equation describing a droplet motion is expressed as follows,

$$m_l \cdot d\mathbf{V}_l / dt = \mathbf{F} + m_l \cdot \mathbf{g} \quad (6)$$

where $\mathbf{F}=(F_x, F_y)$ is a drag force acting on a droplet by the gaseous phase expressed as follows,

$$\mathbf{F} = 1/8 \cdot \pi D^2 \rho (\mathbf{V} - \mathbf{V}_l) |\mathbf{V} - \mathbf{V}_l| C_D \quad (7)$$

where D is the droplet diameter, ρ the gaseous phase density, $m_l = (\pi/6) \cdot D^3 \rho_l$ the droplet mass, ρ_l the droplet density, $\mathbf{V}=(u, v)$ the gaseous phase velocity vector, $\mathbf{V}_l=(u_l, v_l)$ the droplet velocity vector, $\mathbf{g}=(g, 0)$ gravitational acceleration vector. The drag coefficient of a droplet, C_D , is expressed as follows⁽¹²⁾,

$$C_D = 24 / Re_d \cdot (1 + Re_d^{2/3} / 6) \quad (8)$$

where Re_d is a droplet Reynolds number expressed as follows.

$$Re_d = \rho |\mathbf{V} - \mathbf{V}_l| D / \mu \quad (9)$$

One of the most important issues in spray flame simulations is a droplet evaporation model. In the most simplified case, it is assumed that no evaporation occurs prior to saturation temperature of the liquid fuel droplet. In the present study, for estimating the evaporation rate below the saturation temperature, the film theory⁽⁹⁾ was adopted. It is assumed that resistance to the heat and mass exchange between the droplet surface and the gaseous flow is concentrated within an imaginary gas film of constant thickness. To estimate the temperature and the physical properties of the mixture in the film, so-called the 1/3 rule⁽¹³⁾ was used,

$$T_f = T_l + A(T - T_l), \quad Y_{Ff} = Y_{Fs} + A(Y_F - Y_{Fs}) \quad (10)$$

where T_f is reference temperature in the film, T_l the droplet temperature, A the constant factor (=1/3, in this study), T the gaseous phase temperature in the surroundings of the droplet, Y_{Ff} the mass fraction of fuel vapor in the film, Y_{Fs} the mass fraction of fuel vapor at the droplet surface, Y_F the mass fraction of fuel vapor in the surroundings of the droplet. Based on the film theory, the droplet evaporation rate, \dot{m}_l , and the heat transferred to the droplet interior from the gaseous phase, Q_l , are expressed in the following relations⁽⁹⁾, respectively,

$$\dot{m}_l = \pi D \rho_f D_f Sh^* \ln(1 + B_M) \quad (11)$$

$$Q_l = \dot{m}_l \cdot (c_{pFf}(T - T_l) / B_T - L(T_l)) \quad (12)$$

where ρ_f is the mixture density in the film, D_f the mixture diffusion coefficient in the film, c_{pFf} the fuel vapor specific heat at constant pressure in the film, $L(T_l)$ the latent heat of the vaporization at the droplet temperature T_l . B_M is the Spalding's mass transfer number defined as follows.

$$B_M = (Y_{Fs} - Y_F) / (1 - Y_{Fs}) \quad (13)$$

B_T is the Spalding's heat transfer number obtained by the following equations,

$$B_T = (1 + B_M)^\theta - 1 \quad (14)$$

$$\theta = (c_{pFf} / c_{pfl}) \cdot (Sh^* / Nu^*) \cdot (1 / Le_f) \quad (15)$$

where Le_f and c_{pfl} are the Lewis number and the specific heat at constant pressure of the mixture in the film, respectively. Sh^* and Nu^* are the modified Sherwood and Nusselt number of the film, respectively, defined as follows⁽¹⁴⁾.

$$Sh^* = (2 + (1 + Re \cdot Sc)^{1/3} [\max(1, Re_d)]^{0.077} - 1) / F(B_M) \quad (16)$$

$$Nu^* = (2 + (1 + Re \cdot Sc)^{1/3} [\max(1, Re_d)]^{0.077} - 1) / F(B_T) \quad (17)$$

$$F(B) = (1 + B)^{0.7} \ln(1 + B) / B \quad (18)$$

Accordingly, equations describing the diameter and temperature changes of a droplet are expressed as follows,

$$dD / dt = -2\dot{m}_l / \pi D^2 \rho_l \quad (19)$$

$$dT_l / dt = Q_l / (1/6) \cdot \pi D^3 \rho_l c_{pl} \quad (20)$$

where c_{pl} is the specific heat of the liquid fuel droplet.

The source terms, S_l , by interactions between the gaseous and disperse phases are expressed using the total number of droplets, N , existing in each control volume of gaseous phase calculation grid. For the equation of the mass conservation,

$$S_{l,m} = \sum_N \dot{m}_l / \Delta V \quad (21)$$

For the equation of the momentum conservation,

$$S_{l,u} = -\sum_N F_x / \Delta V, \quad S_{l,v} = -\sum_N F_y / \Delta V, \quad (22)$$

For the equation of the energy conservation,

$$S_{l,h} = \sum_N (\dot{m}_l h_F(T) - Q_l - \dot{m}_l (c_{pF}(T - T_l) + L(T_l))) / \Delta V \quad (23)$$

For the equation of the species conservation,

$$S_{l,Y_F} = \sum_N \dot{m}_l / \Delta V \quad (24)$$

where ΔV is volume of the control volume, $h_F(T)$ the specific enthalpy of the fuel vapor at the gaseous phase temperature, T .

For the combustion reaction model, one-step global reaction of n-decane was adopted⁽¹⁵⁾. The source term, $S_{combu,k}$, in the equations of species conservation is expressed using the combustion reaction rate per unit volume, R_F , as follows,

$$S_{combu,k} = -(n_k / n_F)(W_k / W_F) \cdot R_F \quad (25)$$

where n_k is the molar stoichiometric coefficient of the k 's species of the one-step global reaction (positive for the production side), and W_k is the molecular weight of k 's species.

For the calculation, planar symmetry on the central plane ($y = 0$) associated with mirror boundary condition was assumed. The calculation domain ($0 \leq x \leq 20 \text{ mm}$, $0 \leq y \leq 10 \text{ mm}$) was divided into 157×77 equally spaced computational grids in the x and y directions, respectively, (which corresponds to the actual control volume size of $130 \mu\text{m} \times 130 \mu\text{m}$). The calculation time step was 0.1875 ms.

RESULTS and DISCUSSION

Figure 3 and 4 show the calculation results of the flames in case of the size distributions shown in Fig. 2 (a) and (b), respectively. In the figure (a), the gaseous phase velocity vectors, $\mathbf{V} = (u, v)$, superimposed on 2-dimensional profile of the gaseous phase temperature, T , expressed in the gray scale are displayed. In the figure (b), the combustion reaction rate, R_F , expressed in the gray scale and the droplet location and diameter, D , are displayed simultaneously. In the figure (c), gaseous phase equivalence ratio, ϕ , expressed in the gray scale and contours of the stoichiometric ($\phi = 1.0$) are displayed.

Drastic change of flame structure is seen depending on the droplet size distribution. In the flame with larger SMD (Fig. 3), the large droplets penetrate the reaction zone to reach the counter air flow region. In the flame with smaller SMD (Fig. 4), on the other hand, most of the small droplets evaporate before they reach the combustion reaction zone.

Figure 5 shows axial (the x direction) profiles of various quantities, (a) gaseous phase temperature, T , (b) gaseous phase equivalence ratio ϕ , (c) axial velocity, u , and (d) combustion reaction rate, R_F , at $y = 1.0 \text{ mm}$.

In the flame with larger SMD (solid line), twin peaks in the combustion reaction rate are seen on the spray flow side around at $x = 7 \text{ mm}$ (see Fig. 5 (d)). The first peak is located at $x = 7.12 \text{ mm}$ and the second at 7.63 mm (at around the contour of the stoichiometric). As seen in Fig. 3, prevaporization of the droplets occurs before entering the combustion reaction zone and the equivalence ratio shows a maximum of about 0.04 at $x = 5.96 \text{ mm}$ (see Fig. 5 (b)). The first peak of the combustion reaction rate corresponds to the reaction of prevaporized fuel burning in a premixed-combustion mode. Of course, the mixture of $\phi = 0.04$ is not inflammable at ambient temperature. But, in this case, the premixed flame is supported by the heat from high temperature region of the diffusion flame to which the second peak corresponds. The vaporization of droplets in high temperature region behaves like a source of fuel vapor for burning in a diffusion-combustion mode. The value of the second peak of the combustion reaction rate is far bigger than that of the first one. This means that reaction of the diffusion combustion is much

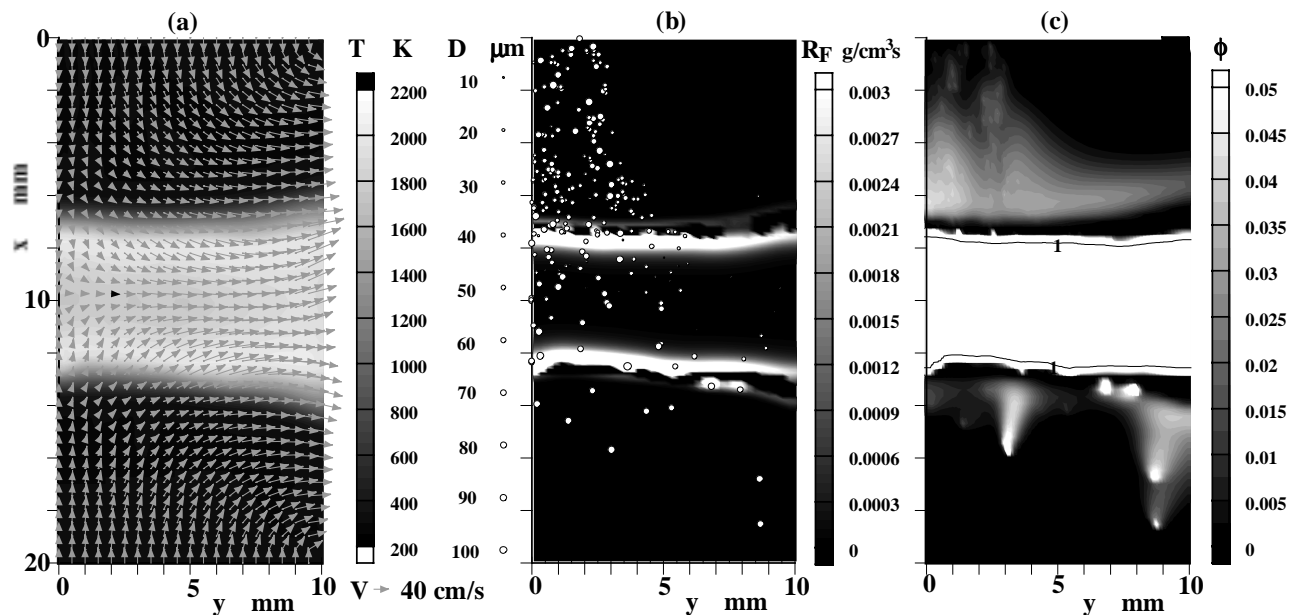


Fig. 3 Calculation results in case of the large droplet size distribution (SMD = 74.2 μm).

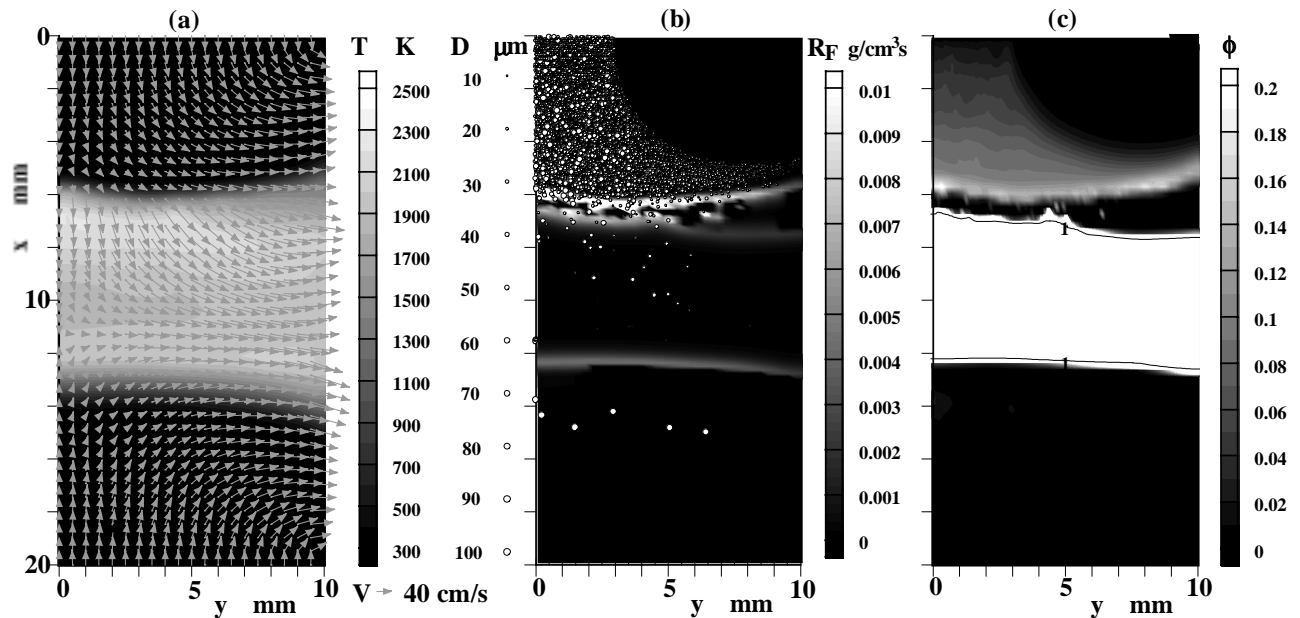


Fig. 4 Calculation results in case of the small droplet size distribution (SMD = 24.8 μm).

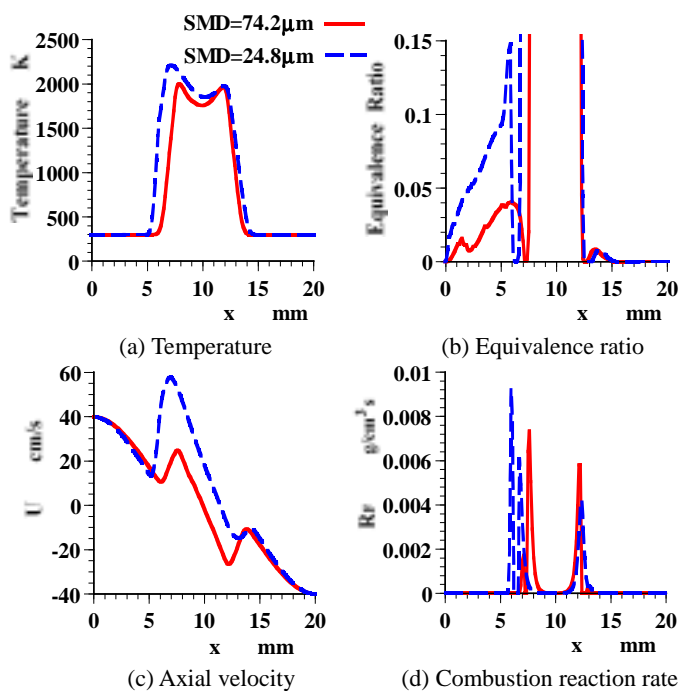


Fig. 5 Axial profiles of various quantities ($y = 1 \text{ mm}$)

more intense than that of the premixed combustion because the vaporization of large droplets does not proceed so much prior to the combustion reaction.

In the flame with smaller SMD (dashed line), twin peaks of the combustion reaction rate are also seen around at $x = 6 \text{ mm}$ (see Fig. 5 (d)). The first peak is located at $x = 5.96 \text{ mm}$ and the second at 6.73 mm (at around the contour of the stoichiometric). As seen in Fig. 4, pre-vaporization is enhanced compared with the former case and the equivalence ratio shows the maximum of about 0.15 at $x = 5.83 \text{ mm}$ (see Fig. 5 (b)). The value of the first peak of the combustion reaction rate is far bigger than that of the second one, which is different from the result of the flame with larger SMD, as shown earlier. This means that reaction of the premixed combustion is much more intense than that of the diffusion combustion due to increase of the pre-vaporised fuel of the small-size spray.

CONCLUSIONS

Numerical calculations of n-decane polydisperse spray flames stabilized in laminar two-dimensional counterflow configuration were conducted by the Eulerian/Lagrangian approach. For the disperse phase, all the individual droplets were tracked without using the concept of "droplet parcel" to discuss the detailed flame structure. Two different droplet size distributions were used for the calculations. As a result, it was found that twin peaks in the combustion reaction rate were seen on the spray flow side of the flames. The first peak corresponded to the reaction of pre-vaporized fuel burning in a premixed-combustion mode. The second peak corresponded to reaction of the fuel vapor generated in high temperature region inside the flame burning in a diffusion-combustion mode. The premixed combustion region was supported by the heat from high temperature region of the diffusion flame. Reaction intensities of the premixed combustion and the diffusion combustion varied depending on the assumed droplet size distribution. This is mainly caused by the fact that pre-vaporization of fuel prior to combustion varies markedly depending on the droplet size distribution.

REFERENCES

- (1) Chiu, H.H., et al., Proc. of Combust. Inst., Vol. 19 (1982), 971.
- (2) Akamatsu F. et al., Atomization and Sprays, 7(1997), 199.
- (3) Mizutani, Y. et al., Mechanics and Combustion of Droplets and Sprays (Ed. H. H. Chiu and N. A. Chigier), (1996), 187, Begell house Inc. NY.
- (4) Akamatsu, F. et al., Proc. of Combust. Inst., Vol. 26 (1996), 1723.
- (5) Wakabayashi, T. et al., 31st Japanese Combustion Symp. (1993), 519.
- (6) Saitoh, H., et al., 2nd Asia-Pacific Conf. on Combust. (1999), 443.
- (7) Kee, R.J., et al., SANDIA Report, SAND87-8215B (1987).
- (8) Kee, R.J., et al., SANDIA Report, SAND86-8246 (1986).
- (9) Abramson, B. and Sirignano, W.A., ASME-JSME Thermal Eng. Joint Conf. (1987), Vol. 1, 11.
- (10) Patankar, S. V., Numerical Heat Transfer and Fluid Flow, (1985), McGraw-Hill.
- (11) Crowe, C. T., et al., Trans. ASME, J. of Fluids Eng., 99 (1977), 325.
- (12) Putnam, A. A., A.R.S. J., 31(1969), p.1467.
- (13) Hubbard, G.L., et al., J. Heat Mass Transfer, 8(1975), 1003.
- (14) Continillo, G. and Sirignano, W.A., Combustion and Flame, 8(1990), 325.
- (15) Westbrook, C.K. and Dryer, F.L., Prog. Ener. Combust. Sci., 10 (1984), 1.